Check for updates

NMR in Biomedicine

WILEY

NMR IN BIOMEDICINE

RESEARCH ARTICLE OPEN ACCESS

Machine Learning Analysis of Single-Voxel Proton MR Spectroscopy for Differentiating Solitary Fibrous Tumors and Meningiomas

Lili Fanni Toth[1] | Carles Majós[2,3] | Albert Pons-Escoda[2] | Carles Arús[1,3] | Margarida Julià-Sapé[1,3]

[1]Departament de Bioquímica i Biologia Molecular and Institut de Biotecnologia i Biomedicina (IBB), Universitat Autònoma de Barcelona (UAB), Barcelona, Spain | [2]Grup de Neuro-Oncologia Institut d'Investigació Biomèdica de Bellvitge (IDIBELL), Hospital Universitari de Bellvitge, Barcelona, Spain | [3]Centro de Investigación Biomédica en Red en Bioingeniería, Biomateriales y Nanomedicina (CIBER-BBN), Spain

Correspondence: Margarida Julià-Sapé (margarita.julia@uab.cat)

Received: 22 November 2024 | **Revised:** 17 March 2025 | **Accepted:** 24 March 2025

Funding: This work was supported by Proyectos de Investigación en Salud 2020, grant numbers PI20/00064 and PI20/00360. Instituto de Salud Carlos III (ISCIII) and Spanish Ministerio de Economía y Competitividad, SAF2014-52332-R. Centro de Investigación Biomédica en Red en Bioingeniería, Biomateriales y Nanomedicina (CIBER-BBN, http://www.ciber-bbn.es/en, accessed April 2, 2025), CB06/01/0010, an initiative of the Instituto de Salud Carlos III (Spain) co-funded by EU Fondo Europeo de Desarrollo Regional (FEDER). Generalitat de Catalunya, Xartecsalut, 2021 XARDI 00021. Lili Tóth was a recipient of the B21P0049 predoctoral fellowship from UAB.

Keywords: machine learning | meningioma | solitary fibrous tumor | spectroscopy

ABSTRACT

Solitary fibrous tumor (SFT), formerly known as hemangiopericytoma, is an uncommon brain tumor often confused with meningioma on MRI. Unlike meningiomas, SFTs exhibit a myoinositol peak on magnetic resonance spectroscopy (MRS). This study aimed to develop automated classifiers to distinguish SFT from meningioma grades using MRS data from a 26-year patient cohort.

Four classification tasks were performed on short echo (SE), long echo (LE) time, and concatenated SE + LE spectra, with datasets split into 80% training and 20% testing sets. Sequential forward feature selection and linear discriminant analysis identified features to distinguish between meningioma Grade 1 (Men-1), meningioma grade 2 (Men-2), meningioma grade 3 (Men-3), and SFT (the 4-class classifier); Men-1 from Men-2 + 3 + SFT; meningioma (all) from SFT; and Men-1 from Men-2 + 3 and SFT. The best classifier was defined by the smallest balanced error rate (BER) in the testing phase.

A total of 136 SE cases and 149 LE cases were analyzed. The best features in the 4-class classifier were myoinositol and alanine at SE, and myoinositol, glutamate, and glutamine at LE. Myoinositol alone distinguished SFT from meningiomas. Differentiating Men-1 from Men-2 was not possible with MRS, and combining higher meningioma grades did not improve distinction from Men-1. Notably, combining short and long echo times (TE) enhances classification performance, particularly in challenging outlier cases. Furthermore, the robust classifier demonstrates efficacy even when dealing with spectra of suboptimal quality. The resulting classifier is available as Supporting Information of the publication. Extensive documentation is provided, and the software is free and open to all users without a login requirement.

Abbreviations: BER, balanced error rate; FWHM, full width at half maximum; Glx, glutamate and glutamine; HLSVDPRO, Hankel–Lanczos singular value decomposition with partial reorthogonalization; LDA, linear discriminant analysis; Men-1, meningioma grade 1; Men-2, meningioma grade 2; Men-3, meningioma grade 3; MRS, magnetic resonance spectroscopy; NAA, N-acetylaspartate; PCA, principal component analysis; SFFS, sequential forward feature selection; SFT, solitary fibrous tumor; SNR, signal-to-noise ratio; SV, single voxel; WHO, World Health Organization.

This is an open access article under the terms of the Creative Commons Attribution-NonCommercial-NoDerivs License, which permits use and distribution in any medium, provided the original work is properly cited, the use is non-commercial and no modifications or adaptations are made.

© 2025 The Author(s). *NMR in Biomedicine* published by John Wiley & Sons Ltd.

1 | Introduction

Solitary fibrous tumor (SFT), previously termed hemangiopericytoma, is a rare mesenchymal tumor accounting for < 1% of all primary central nervous system tumors. The nomenclature and classification of SFTs have changed over time, reflecting an evolving understanding of these tumors as additional information has been uncovered through research and clinical studies [1, 2]. Preoperative diagnosis of SFTs is crucial due to their aggressive nature, elevated local recurrence rate, and tendency for late distant metastases [3].

As of today, SFT is often poorly recognized presurgically and remains a diagnostic challenge [4, 5]. Due to its rarity and resemblance to meningioma, SFT is usually misdiagnosed as meningioma on imaging, and the actual diagnosis is often not suspected until confirmed with postsurgical histopathology [6, 7]. Previous studies have compared the value of metabolites measured by magnetic resonance spectroscopy (MRS) between SFT (formerly termed hemangiopericytoma) and meningioma [8, 9]. The characteristic metabolites associated with meningioma include notably elevated choline levels, the presence of alanine, glutamate and glutamine (Glx), and minimal to undetectable N-acetylaspartate (NAA) and creatine [10–12]. Studies carried out with three hemangiopericytomas and five SFT cases, respectively [8, 9], described high levels of myoinositol.

On the other hand, the distinction among the different grades and subtypes of meningiomas is challenging based on conventional MRI [4, 7]. This may be of relevance because meningioma of Grade 2 (Men-2) has a 40% risk of recurrence if untreated [13], in contrast with Grade 1 (Men-1). In this respect, using the WHO 2000 classification on radiological reports of conventional MRI, one study found sensitivities of 100% for low-grade meningioma and 0% for high-grade meningioma in a retrospective multicenter cohort of 393 patients [14]. Moreover, a study from 2020 found similar sensitivities (93.7%, low-grade meningioma and 17.2, high-grade meningioma) [15]. Recent studies using other MRI cohorts have proposed methods to distinguish between low- and high-grade meningiomas, usually by also aggregating Grades 2 and 3 [16–18] with variable success.

Most previous studies using MRS for distinguishing SFT and meningioma involved a small number of cases, particularly for SFT, or the software used for data processing [19] is no longer receiving updates, highlighting the need for conducting research with expanded datasets and reproducible methodologies to confirm and validate these findings.

Therefore, the main aim of this work was the retrospective analysis of single-voxel (SV) MRS, to extract and assess a combination of features, allowing us to develop novel tools to improve diagnosis of SFT and the refinement of the classification of meningioma grades, using a single-center, retrospective cohort of meningioma, and SFT from the period spanning from 1997 to 2023. A secondary aim was to evaluate the effect of spectral quality in the MRS-based classification.

2 | Materials and Methods

2.1 | Patient Selection and Inclusion Criteria

SV MRS data were collected at *Hospital de Bellvitge*, Spain, between 1997 and 2023. The dataset contains 231 SV spectra acquired from two models of 1.5 T MR scanners, Philips Intera and 1.5 T and 3 T Philips Ingenia. The parameters of the acquisition conditions are summarized in Table 1. From the internal records of the *Hospital de Bellvitge*, cases were selected for training given that they met the following inclusion criteria:

1. Diagnosis of Men-1, Men-2, meningioma grade 3 (Men-3), or SFT, according to the World Health Organization (WHO) classification of brain tumors 2021 [1, 20].
2. At least one SV MRS acquisition at one echo time (TE) available.
3. Both water-suppressed and water-unsuppressed spectra available.
4. The spectra can be opened with jMRUI versions 4, 5, or 6 [21].
5. Phase correction can be performed using the corresponding water-unsuppressed file.
6. Entire processing pipeline can be accomplished using jMRUI2XML [22, 23].
7. Signal-to-noise (SNR) ratio greater than 10 [24].
8. The full width at half maximum height (FWHM) should be less than 8 Hz [24].

2.2 | Data Processing

Spectra were first opened with jMRUI versions 4, 5, or 6, depending on the acquisition year and format and converted into jMRUI format. Subsequently, each water-suppressed file's phase was corrected by dividing it with the water-unsuppressed file. The spectra then were opened with the jMRUI2XML plugin [22, 23] of jMRUI version 6.0 [21]. The jMRUI2XML plugin processed the data, using the INTERPRET [25] parameters, as follows: First, the water reference peak was set at 4.75 ppm, then Lorentzian apodization with 1 Hz was applied. Subsequently, the remnant water signal within the range of 4.31–5.11 ppm was filtered out. For this, the 4.2- to 5.1-ppm region was set to zero so that any remnant unsuppressed water does not interfere with the normalized peak heights of the relevant metabolite signals. This was followed by baseline correction in two distinct regions (9.0 to 11.0 ppm and −2.0 to −1.0 ppm). Finally, the spectra were aligned, including a priority order for alignment correction of 3.03 ppm, followed by 3.21 ppm, and then 1.29 ppm [22]. After performing these steps, each spectrum was exported in XML format, yielding XML files with 512 data points spanning the range from −2.7 ppm to 7.1 ppm.

Quality control parameters were calculated in the following way: FWHM was calculated from the water unsuppressed spectra with Hankel–Lanczos Singular Value Decomposition

10991492, 2025, 5, Downloaded from https://analyticalsciencejournals.onlinelibrary.wiley.com/doi/10.1002/nbm.70032 by Fundació I·CERCA Fundació Institució Centres de Recerca de Catalunya, Wiley Online Library on [10/06/2025]. See the Terms and Conditions (https://onlinelibrary.wiley.com/terms-and-conditions) on Wiley Online Library for rules of use; OA articles are governed by the applicable Creative Commons License

TABLE 1 | Summary of the acquisition parameters used in the dataset.

Study parameter	Information provided in this manuscript
a. Field strength	1.5 and 3.0 T (1 case of Men-1 recorded at 3 T used in the classifiers)
b. Manufacturer	Philips Medical Systems
c. Model	1.5 T: Achieva dStream/GIyroscan/Intera 3 T: Ingenia
d. RF coil	• Achieva dStream → transmit: body; receive: synergy • Ingenia: ◦ Transmit: Body/Surface ◦ Receive: NVC-base, NVC-head, NVC-head/neck, dsHead-32channels • Intera: ◦ Transmit: surface ◦ Receive: head/volume
e. Additional hardware	None
a. Pulse sequence	PRESS
b. Volume of interest (VOI)	Not mentioned
c. Nominal VOI size	3–8 cm^3
d. TE/TR	SE: 30–32 ms and LE: 135–136 ms TR almost entirely 2000 ms
e. Number of samples acquired (NSA)	513 and 1024
f. Additional parameters (BW, frequency offsets, 2D or 3D, matrix size, acceleration factors, and sampling method)	BW: 1000 or 2000 Hz Points: 512 Unsuppressed water acquisition Suppressed water acquisition
g. Water suppression method	Not mentioned
h. Shimming method and thresholds	Not mentioned
i. Triggering or motion correction method	Not mentioned
a. Analysis software	jMRUI with the jMRUI2XML plugin and SpectraClassifier
b. Processing steps deviating from quoted reference or product	Frequency alignment was performed over (in order of priority): 3.03, 3.21, and 1.29 ppm
c. Output measure (e.g., absolute concentration, institutional units, and ratio), processing steps deviating from quoted reference or product	Class
d. Quantification references and assumptions, fitting model assumptions	N/A
a. Reported variables (SNR, linewidth with reference peaks)	FWHM with water reference at 4.75 ppm SNR = (maximum intensity in [2.7–7.1]) / (2·SD noise in [2.7–7.1])
b. Data exclusion criteria	Excluded if SNR < 10 and FWHM > 8 Hz
c. Quality measures of postprocessing model fitting (e.g., CRLB, goodness of fit, and SD of residuals)	N/A Thresholds of intensities on the y-axis of −0.025 for SE and −0.2 for LE were applied in the range of −2.7–7.1 ppm to filter out spectra containing potentially artifactual negative intensity values
d. Sample spectra	Figures 2–5

with Partial ReOrthogonalization (HLSVDPRO) [26, 27] for one component, and SNR was calculated by jMRUI2XML [22]. Additionally, thresholds of intensities on the y-axis of −0.025 for SE and −0.2 for LE were applied in the range of −2.7–7.1 ppm to filter out spectra containing potentially artifactual negative intensity values.

10991492, 2025, 5, Downloaded from https://analyticalsciencejournals.onlinelibrary.wiley.com/doi/10.1002/nbm.70032 by Fundació I·CERCA Fundació Institució Centres de Recerca de Catalunya, Wiley Online Library on [10/06/2025]. See the Terms and Conditions (https://onlinelibrary.wiley.com/terms-and-conditions) on Wiley Online Library for rules of use; OA articles are governed by the applicable Creative Commons License

2.3 | Classification Tasks

Classifiers were trained on 80% of the data and tested on the remaining 20%, with cases shuffled for randomization. Distribution of cases in each dataset is available in Table 2.

Four classification questions were performed:

Four-class task:

A. Men-1 versus Men-2 versus Men-3 versus SFT: Is it possible to simultaneously separate SFT and identify different grades of meningioma?

Two-class task:

B. Meningioma (all grades) versus SFT: Can fibrous solitary tumor be distinguished from meningiomas?

C. Men-1 versus Men-2: Can we distinguish between Grade 1 and Grade 2 meningiomas?

Three-class task:

D. Men-1 versus Men-2 + 3 (Men-2 and Men-3) versus SFT: Is it possible to simultaneously separate SFT from low risk of recurrence meningioma and high risk of recurrence meningioma?

Each task was performed on the SE, LE, and concatenated SE + LE spectra (as in [28]), yielding 12 classification tasks in total.

2.4 | Feature Selection and Classification

The feature selection and classification steps were implemented using the SpectraClassifier program [29]. Feature selection methods used were sequential forward feature selection (SFFS) and principal component analysis (PCA), from 1 to 20 features or components. PCA was set to cover 95% of variance. Classification was performed using linear discriminant analysis (LDA).

2.5 | Classifier Evaluation

Classifier performance was evaluated using the balanced error rate (BER), area under the receiver operating characteristic curve (AUC), and the F1-score for both training and testing phases. For Questions A and D, we calculated the macro F1-scores. Best performance was defined as the smallest testing phase BER. Differences in AUCs were tested with the Hanley–McNeil test (significance level: 0.05). Secondary analysis included previously discarded low-quality spectra as a test set to evaluate data quality impact.

2.6 | Handling Limited Test Cases

To address the limited number of cases in the test sets, we trained classifiers using the entire dataset and evaluated them through bootstrapping and fivefold cross-validation. Details on the extracted features and classifier evaluations are provided in the Supporting Information.

3 | Results

Figure 1 shows the results of applying the inclusion criteria. Out of the initial 231 potential cases, 137 were female (Men-1: 109, Men-2: 25, Men-3: 2, and SFT: 1), and 93 were male (Men-1: 71, Men-2: 17, Men-3: 1, and SFT: 4); one did not specify gender. The mean cohort age is 58.5 ± 13.90 years. Average ages for females were Men-1: 57.9 ± 13.5, Men-2: 62.7 ± 12.6, Men-3: 71.0 ± 11.3, and SFT: 65.0 ± 0.00 and for males: Men-1: 57.3 ± 14.3, Men-2: 63.4 ± 13.4, Men-3: 45.0 ± 0.00, and SFT: 42.0 ± 15.8. Figure 2 shows the average spectra for each tumor type for the two echo times. Key differences include a large peak around 3.55 ppm in the SE spectra of SFTs, which is absent in the meningioma group, the absence of the inverted alanine doublet ca. 1.4 ppm in SFTs at LE, and low Glx resonances (ca. 2–2.2 ppm) at both TE in SFT.

The processed SFT spectra are shown in Figure 3, revealing variability in spectral patterns. At SE, myoinositol at 3.57 ppm is prominent in Case 215, while other cases show varying myoinositol/choline ratios. At LE, choline at 3.21 is predominant with additional signals like creatine and N-acetyl containing compounds [30] (NAA is usually undetectable in extracts of SFTs [8]).

3.1 | Classification Results

The selected features of the classifiers are summarized in Table 3, while performance metrics are summarized in Table 4. The best results for most tasks were achieved through feature selection using SFFS followed by classification by LDA. An exception is Question C, where the BER with PCA at LE is smaller (0.268) than with SFFS (0.542), although the SE + LE model yields better results. Similarly, Question D shows lower BER values in the LE train and test sets, but the best model is achieved with LE + SE. Further details about the selected features can be found in the Supporting Information.

3.1.1 | Question A: Men-1 Versus Men-2 Versus Men-3 Versus SFT

For Question A, BER values for test cases could not be calculated due to a limited number of SFT and Men-3 cases. The lowest BER in the training phase is achieved with SE (Table 4). AUC for SFT is 1.000 for the training test set and 0.990 for Men-3. For Men-1 and Men-2, performance is lower (0.865 and 0.763, respectively, in the training, and 0.557 and 0.753 in the test). The selected features are 3.571 (likely corresponding to the doublet-of-doublets of myoinositol centered at 3.52 ppm, that strongly decreases at LE), 3.495 (likely corresponding to contributions from the taurine triplet centered at 3.42 and/or the D-glucose multiplet at 3.43 ppm), and 1.404 ppm (likely corresponding to the alanine doublet centered at 1.47 ppm) [31]. The first feature (3.571 ppm) is the same as the single feature selected in Question B, indicating that it is related to SFTs. For LE, performance in terms of AUC for SFT slightly decreases (0.923 training), with the classifier using a feature

10991492, 2025, 5, Downloaded from https://analyticalsciencejournals.onlinelibrary.wiley.com/doi/10.1002/nbm.70032 by Fundació Institució Centres de Recerca de Catalunya, Wiley Online Library on [10/06/2025]. See the Terms and Conditions (https://onlinelibrary.wiley.com/terms-and-conditions) on Wiley Online Library for rules of use; OA articles are governed by the applicable Creative Commons License

TABLE 2 | Distribution of cases in training and test set for short echo (SE) and long echo (LE) spectra. Quality parameters split by echo time (short or long), set (training or test), and class. FWHM in hertz, SNR calculated as in [22]. Median and standard deviation. * As can be seen from the upper value of the range, one SFT had an FWHM higher than 8 Hz. We decided to include this case in the analysis since the spectra visually appeared to be of good quality.

Echo time	Set		Men-1	Men-2	Men-3	SFT
SE	Train	Cases	79	23	2	4
		FWHM	4.88 (2.4–7.97)	4.90 (2.86–6.06)	6.42 (5.19–7.65)	5.49 (3.78–9.08
		SNR	41.5 (10.3–142)	61.0 (15.6–156)	41.9 (34.0–49.8)	72.2 (65.4–102)
	Test	Cases	24	3	0	1
		FWHM	4.77 (3.80–661)	4.75 (2.71–77.9)	—	4.36
		SNR	46.7 (19.4–142)	71.10 (14.4–131)	—	49.7
LE	Train	Cases	91	22	2	4
		FWHM	4.78 (1.93–7.98)	4.68 (2.73–7.22)	6.58 (5.11–8.05)	5.04 (3.56–7.72)
		SNR	48.6 (10.2–314)	48.0 (10.6–164)	32.0 (23.3–40.7)	62.2 (45.0–124)
	Test	Cases	21	8	0	1
		FWHM	4.77 (3.80–6.61)	4.75 (2.71–7.79)	—	4.36
		SNR	46.7 (19.4–142)	71.0 (14.4–49.7)	—	49.7
SE + LE	Train	Cases	66	21	2	4
		FWHM	4.73 (1.93–7.98)	4.75 (2.73–6.06)	6.42 (5.11–8.05)	5.49 (4.36–9.08)*
		SNR	44.9 (10.3–198)	59.6 (15.06–156)	37.3 (23.3–49.8)	65.5 (45.0–124)
	Test	Cases	21	2	0	1
		FWHM	4.83 (2.30–7.97)	4.83 (4.58–5.85)	—	3.67 (3.56–3.78)
		SNR	52.1 (22.3–314)	57.1 (48.7–93.4)	—	70.6 (62.3–78.9)

related to the myoinositol peak (3.514 ppm), and other two features. One of them is 2.190 ppm, likely corresponding to Glx (Figure 2), where it can be observed that neither of the classes displays a NAA peak, in accordance with previous literature [8, 12]. The other feature was 4.108 ppm, which may have contributions from the lactate CH methine or from one of the myoinositol resonances. Additionally, there may be a contribution from the incomplete water suppression and related to the remnants of the water peak tail. For the SE + LE, two features are extracted from the SE dataset, 3.533 is again related to the myoinositol peak, and 2.152 likely corresponding to the Glx peaks range. The third feature comes from the LE dataset, 3.015 ppm is indicative of creatine (3.03 ppm). Notably, the classifier trained with LE performs the least effectively.

3.1.2 | Question B: Meningioma (All Grades) Versus SFT

For Question B, all yielded low BERs, noteworthy 0.019 and 0.000, respectively, in the SE and LE and test sets. Additionally, the AUC values were especially high (SE train: 0.999, LE train: 0.886, SE + LE train: 1.000). While the SE + LE combined data demonstrated the highest AUC, it is important to note that statistical analysis of AUC (Hanley–McNeil test, $p < 0.001$) revealed no significant differences when compared to the SE model.

The extracted features of 3.571 ppm (SE) and 3.533 ppm (SE + LE) are due to the doublet of myoinositol centered at 3.52 ppm. Cases 23 and 36, both Men-1, are misclassified in the SE and SE + LE training set and test set, respectively, but notably, Case 36 is classified correctly in the test set when using a combination of SE and LE data (Figure 4). Based on this model, we developed a prototype decision support system featuring a user-friendly graphical interface, allowing clinicians to easily calculate the intensity at 3.571 ppm and accurately classify MRS spectra as either SFT or meningioma according to the classification equation from our results. The tool, along with detailed instructions, is available as Supporting Information and in [32].

3.1.3 | Question C: Men-1 Versus Men-2

For Question C, the SE dataset yielded the lowest BER values of 0.375 in the test set but looking at the AUC values (0.319) in the test set, while the model might have low BER, it struggles to effectively discriminate between the two classes. The SE + LE model yielded a BER of 0.440 in the testing set, but the AUC value of 0.642 is higher than in the case of only using SE. This model contains one feature (1.404 ppm) from the SE data, likely corresponding to the alanine doublet centered at 1.47 ppm and six other features (2.938, 2.996, 3.015, 3.053, 3.072, and 3.111 ppm) all centered around the creatine peak.

10991492, 2025, 5, Downloaded from https://analyticalsciencejournals.onlinelibrary.wiley.com/doi/10.1002/nbm.70032 by Fundació Institució Centres de Recerca de Catalunya, Wiley Online Library on [10/06/2025]. See the Terms and Conditions (https://onlinelibrary.wiley.com/terms-and-conditions) on Wiley Online Library for rules of use; OA articles are governed by the applicable Creative Commons License

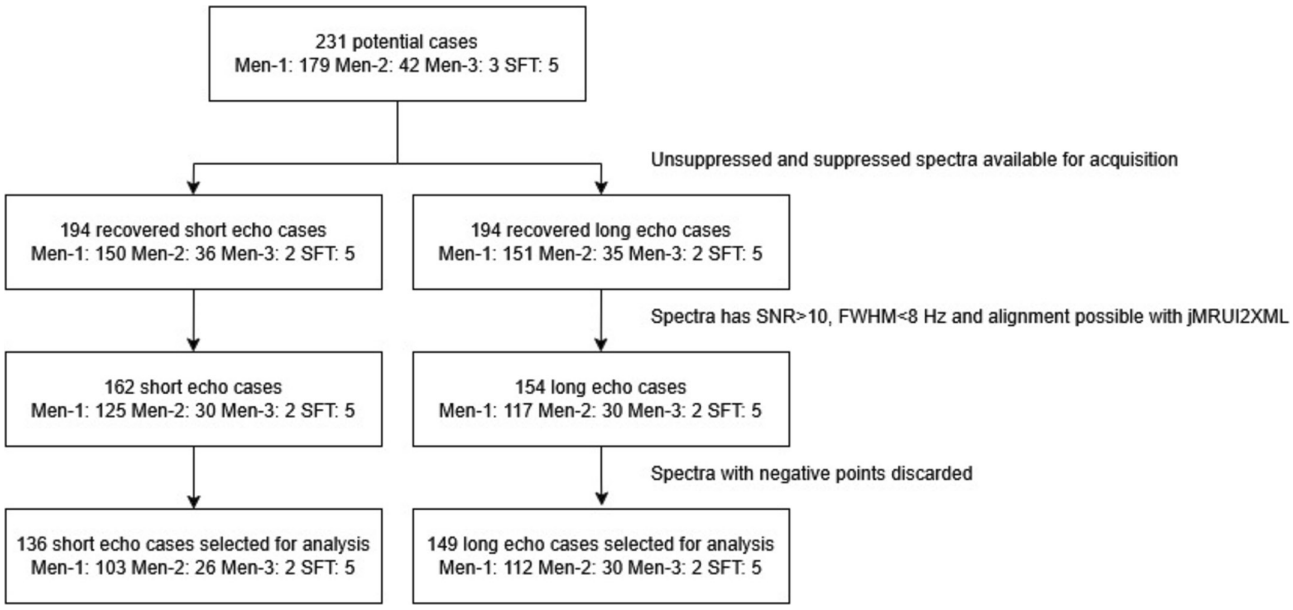

FIGURE 1 | Results of applying the inclusion criteria; spectra with potentially artifactual negative peaks were discarded.

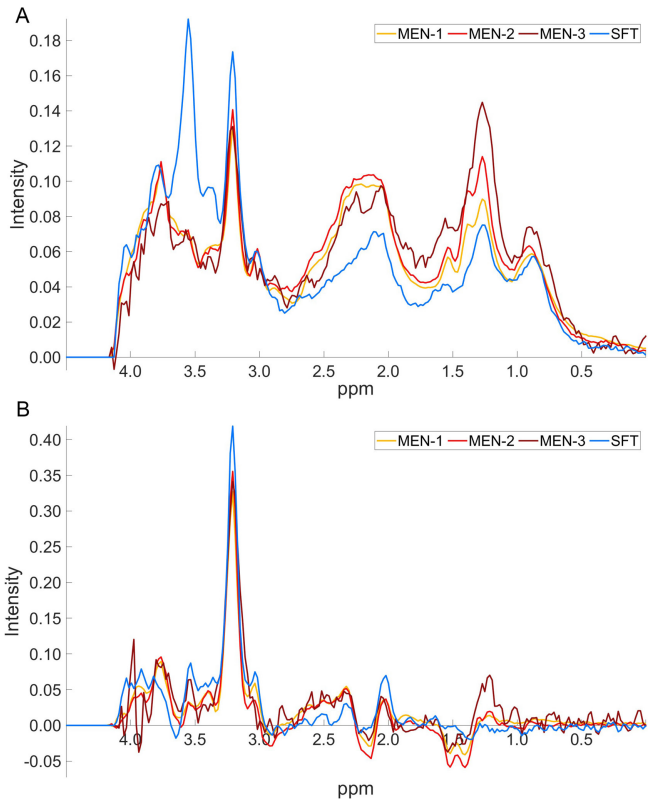

FIGURE 2 | Mean spectra of each tumor type. (A) Short echo (SE) spectra (meningioma grade 1 (Men-1): 103, meningioma grade 2 (Men-2): 26, meningioma grade 3 (Men-3): 3, solitary fibrous tumor (SFT): 5. (B) Long echo (LE) spectra (Men-1: 112, Men-2: 30, Men-3: 3, and SFT: 5).

Looking at the SE and LE classifiers, there are no significant differences neither between the training (Hanley–McNeil test, $p = 0.888$) nor between the test sets (Hanley–McNeil test, $p = 0.601$). The first two features of those two other models are 1.519 ppm (SE) and 0.599 ppm (LE). The other five features (SE: 4.012, 4.032, 4.051, 4.070, 4.089, 4.108 ppm, LE: 4.012, 4.032, 4.051, 4.070, 4.081, and 4.108 ppm) are almost identical, indicating that these features are probably related as above, to incomplete water suppression, myoinositol, and/or lactate contributions. Also, one particular aspect regarding the correlative selection of features is that when the SpectraClassifier software does SFFS, it starts by the end (from 4.1 ppm in its default mode); the criterion is correlation-based. When successive features near 4.1 ppm are chosen, it means that in fact all features are more or less equally important by the internal feature quality criterion, in sequential forward mode from 4.1 ppm. This provides further evidence of the low discriminative capacity of the classifier.

3.1.4 | Question D: Men-1 Versus Men-2 and Men-3 Versus SFT

Question D aims to address whether pooling together the higher grade meningiomas improves the classification. In comparison to Question A, the lower BER values are achieved by combining the two echo types. The first feature of both the SE and SE + LE model are 3.571 and 3.533 ppm, respectively, and is indicative of SFT, which both models can identify quite well. The second feature varies in the models, but in the case of the combined echo types, it is 3.015 ppm (creatine), which is a feature which was also present in the model for Question C.

The second feature extracted in both the SE and SE + LE cases corresponds to the features (SE: 3.495 ppm, SE + LE: 3.105 ppm [LE]) identified in Question A. However, in the case of LE, the features differ from those in Question A, yet they are the same as the features observed in Question C. This suggests a probable association with incomplete water suppression in these features.

Looking at the AUC values of each class in Table 4, we can see that the identification of Men-1 decreases in this situation in

10991492, 2025, 5, Downloaded from https://analyticalsciencejournals.onlinelibrary.wiley.com/doi/10.1002/nbm.70032 by Fundació I-CERCA Fundació Institució Centres de Recerca de Catalunya, Wiley Online Library on [10/06/2025]. See the Terms and Conditions (https://onlinelibrary.wiley.com/terms-and-conditions) on Wiley Online Library for rules of use; OA articles are governed by the applicable Creative Commons License

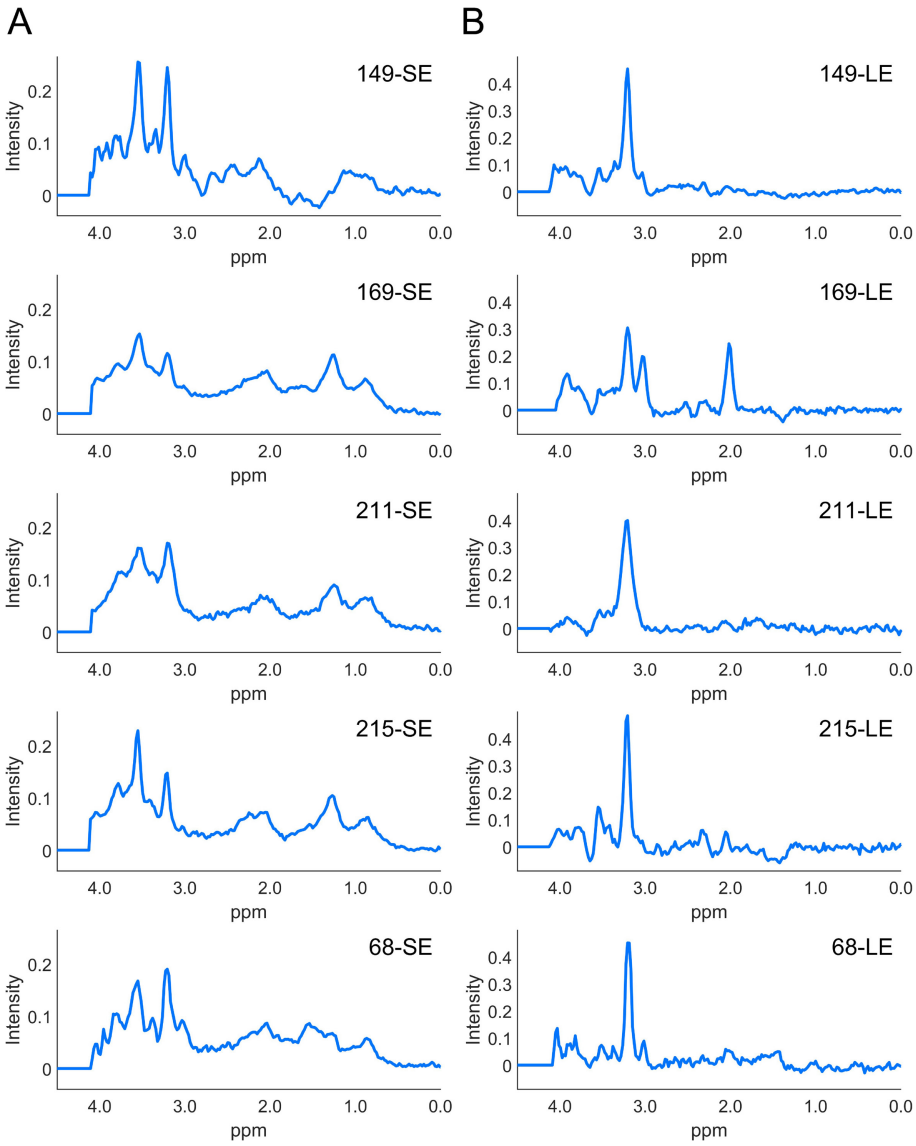

FIGURE 3 | Processed SFT spectra at short echo (SE) and long echo (LE). Last row: testing set. The anonymized case number is the numeric value before the "-SE" and "-LE" tags, which indicate the echo type (e.g., nn-[LE/SE]).

the training phase, but it is not statistically significant (Train: $p = 0.1720$, Test: $p = 0.8328$).

3.2 | Classifier Robustness Against Bad Quality Data

The spectra that did not meet the previously outlined requirements and were excluded from the analysis ($n = 21$) are shown in Figure 5. To assess the robustness of our classifiers, we used these discarded, suboptimal quality spectra as an additional test set. Detailed results can be found in the Supporting Information. The most relevant finding was that for Question B (meningioma vs. SFT), 97% of all meningiomas at SE and 100% using both echo times were correctly classified, while only 29.0% of meningiomas were correctly assigned as meningioma by the LE classifier (Figure 6). For Question A, the performance is comparable to that of the original test set; however, for the other two questions (C and D), the classifier's performance is noticeably impacted.

4 | Discussion

This work aimed to analyze SV MRS for effectively distinguishing SFT from meningiomas and improve the classification of meningioma grades, utilizing a single-center, retrospective cohort of meningioma, and SFT spanning from 1997 to 2023.

Our findings show that classifiers trained on SE data effectively distinguish SFT from meningiomas. The singular feature extracted (3.571 ppm) closely aligns with the major myoinositol peak (3.52 ppm), often elevated in SFTs, according to prior studies [8, 9]. Notably, classifiers exclusively trained with LE data exhibit reduced predictive performance, likely attributable to the low visibility of myoinositol in LE spectra. According to our results, SFT may be confidently suspected when a large peak at 3.52 ppm is found on a SE spectrum of an extra-axial tumor. This finding is in agreement with previous reports, as stated in Section 1 [8, 9].

10991492, 2025, 5, Downloaded from https://analyticalsciencejournals.onlinelibrary.wiley.com/doi/10.1002/nbm.70032 by Fundació I-CERCA Fundació Institució Centres de Recerca de Catalunya, Wiley Online Library on [10/06/2025]. See the Terms and Conditions (https://onlinelibrary.wiley.com/terms-and-conditions) on Wiley Online Library for rules of use; OA articles are governed by the applicable Creative Commons License

TABLE 3 | Properties of models with lowest BER rates in training phase, including selected features and classification methods across datasets. Feature origin noted in brackets, short echo (SE), or long echo (LE).

Classification task	Dataset	Number of features	Feature selection	Classification	Selected features (ppm)						
Question A: Men-1 versus Men-2 versus Men-3 versus SFT	SE	3	SFFS	LDA	3.571	3.495	1.404				
	LE	3	SFFS	LDA	3.514	2.190	4.108				
	SE + LE	3	SFFS	LDA	3.533 (SE)	3.015 (LE)	2.152 (SE)				
Question B: meningioma versus SFT	SE	1	SFFS	LDA	3.571						
	LE	1	SFFS	LDA	2.401						
	SE + LE	1	SFFS	LDA	3.533 (SE)						
Question C: Men-1 versus Men-2	SE	7	SFFS	LDA	1.519	4.012	4.032	4.051	4.070	4.089	4.108
	LE	7	SFFS	LDA	0.599	4.012	4.032	4.051	4.070	4.081	4.108
	SE + LE	7	SFFS	LDA	1.404 (SE)	2.938 (LE)	2.996 (LE)	3.015 (LE)	3.053 (LE)	3.072 (LE)	3.111 (LE)
Question D: Men-1 versus Men2 + 3 versus SFT	SE	2	SFFS	LDA	3.571	3.495					
	LE	2	SFFS	LDA	4.109	4.090					
	SE + LE	2	SFFS	LDA	3.533 (SE)	3.015 (LE)					

10991492, 2025, 5, Downloaded from https://analyticalsciencejournals.onlinelibrary.wiley.com/doi/10.1002/nbm.70032 by Fundació Institució Centres de Recerca de Catalunya, Wiley Online Library on [10/06/2025]. See the Terms and Conditions (https://onlinelibrary.wiley.com/terms-and-conditions) on Wiley Online Library for rules of use; OA articles are governed by the applicable Creative Commons License

TABLE 4 | AUC and BER values for training and test sets. Shaded rows highlight the lowest testing BER. N/A indicates cases where the value could not be calculated due to missing true positive instances in the test set.

Question	Set		AUC		BER	
A) Men-1 versus Men-2 versus Men-3 versus SFT			Train	Test	Train	Test
	SE	Men-1	0.865 ± 0.040	0.557 ± 0.665	0.214	N/A
		Men-2	0.763 ± 0.099	0.753 ± 0.102		
		Men-3	0.990 ± 0.000	N/A		
		SFT	1.000 ± 0.000	N/A		
	LE	Men-1	0.577 ± 0.063	0.624 ± 0.062	0.554	N/A
		Men-2	0.691 ± 0.117	0.639 ± 0.124		
		Men-3	0.715 ± 0.000	N/A		
		SFT	0.923 ± 0.163	N/A		
	SE + LE	Men-1	0.735 ± 0.061	0.674 ± 0.066	0.232	N/A
		Men-2	0.691 ± 0.116	0.749 ± 0.107		
		Men-3	0.910 ± 0.000	N/A		
		SFT	1.000 ± 0.000	N/A		
B) Meningioma versus SFT	SE		0.999 ± 0.000	N/A	0.004	0.019
	LE		0.886 ± 0.029	N/A	0.169	0.103
	SE + LE		1.000 ± 0.000	N/A	0.006	0.000
C) Men-1 versus Men-2	SE		0.782 ± 0.051	0.319 ± 0.067	0.308	0.375
	LE		0.772 ± 0.049	0.505 ± 0 0.069	0.256	0.542
	SE + LE		0.879 ± 0.042	0.666 ± 0.076	0.201	0.440
D) Men-1 versus Men2 + 3 versus SFT	SE	Men-1	0.762 ± 0.053	0.687 ± 0.060	0.229	0.403
		Men2 + 3	0.744 ± 0.099	0.660 ± 0.111		
		SFT	0.999 ± 0.000	N/A		
	LE	Men-1	0.529 ± 0.069	0.621 ± 0.069	0.565	0.696
		Men2 + 3	0.606 ± 0.116	0.548 ± 0.119		
		SFT	0.593 ± 0.316	N/A		
	SE + LE	Men-1	0.771 ± 0.056	0.698 ± 0.064	0.213	0.190
		Men2 + 3	0.764 ± 0.104	0.568 ± 0.135		
		SFT	1.000 ± 0.000	N/A		

Initially, two meningioma cases (Case 23 in training, Case 36 in testing) are misclassified as SFTs when using SE. However, when combining the two echo times, Case 36 is correctly classified. While both cases met the SNR and FWHM constraints, visual inspection of Figure 4 reveals other indicators of an uncommon spectral pattern in Case 23. For example, the lack of a prominent choline peak, which is expected in classical meningiomas. Comparing the spectra of these two cases to the average spectra of their respective tumor type clearly shows their visual differences (Figure 4). This pattern of misclassification underscores the importance of spectral quality. Similarly, Figure 3 shows variability among the SFT spectra. In the SE spectra, we observe myoinositol and varying levels of choline. In the LE spectra, choline at 3.21 ppm is the most prominent peak. Case 169 is a notable outlier, as it also exhibits additional signals, including creatine and N-acetyl-containing compounds. Since NAA is typically undetectable in extracts of SFTs, as described in [8], the presence of these peaks may suggest that the patient moved during acquisition, leading to spurious signals. Although we confirmed the voxel location at both echo times, according to the headers of the corresponding files and the accompanying MRI series are not artifactual, we cannot rule out that the patient moved during the acquisition [33].

Although SFTs are rare, these findings may be highly relevant on daily clinical practice. SFT are mainly reported as extra-axial tumors and difficult to distinguish from meningiomas with conventional imaging alone. In fact, these tumors are often

10991492, 2025, 5, Downloaded from https://analyticalsciencejournals.onlinelibrary.wiley.com/doi/10.1002/nbm.70032 by Fundació I+CERCA Fundació Institució Centres de Recerca de Catalunya, Wiley Online Library on [10/06/2025]. See the Terms and Conditions (https://onlinelibrary.wiley.com/terms-and-conditions) on Wiley Online Library for rules of use; OA articles are governed by the applicable Creative Commons License

confounded with meningioma presurgically. Nevertheless, SFT is an aggressive tumor requiring prompt surgical resection and complementary radiation therapy treatment, different to Men-1, which, depending on patient symptoms, could be conservatively managed with follow-up due to low or absent growth tendency on follow-up. Thus, from our results, we deduce that when a neuroradiologist identifies an extra-axial tumor resembling a meningioma on imaging, MRS using SE should be performed. If a myoinositol peak is detected, there should be a strong consideration of a SFT, potentially needing expedited surgical resection.

The datasets have a limited number of Men-3 and SFT cases, however, the low numbers reflect the rarity of SFTs and Men-3, which prevalence is one new case per million people per year [34]. To our knowledge, the data described here belong to the largest SFT/meningiomas datasets reported in the literature [9].

In comparison to a similar study by Ohba et al. [9], which included 84 patients (72 Men-1, 7 Men-2, and 5 SFT) aged 16–86 (69% female, 31% male), our study confirms the relevance of myoinositol in distinguishing SFTs from meningiomas. However, while Ohba et al. identified an association between SFT and age < 45 years, our SFT patients have an average age of 46.5, with two individuals surpassing the age of 45 (64 years in male patient 169 and 65 years in female patient 68). We attribute the discrepancy to the fact that all SFT patients in Ohba et al.

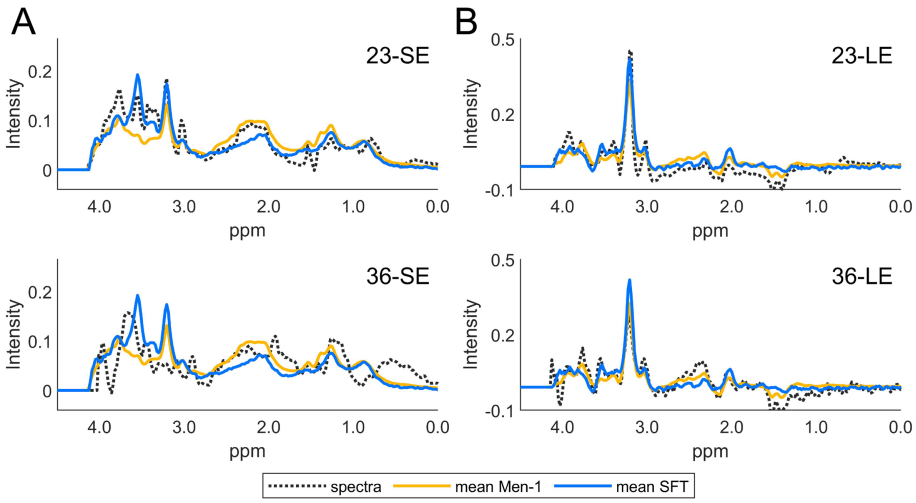

FIGURE 4 | Comparison of spectra from misclassified cases and mean spectra of meningioma grade 1 (Men-1) and solitary fibrous tumor (SFT). (A) Short echo (SE). (B) Long echo (LE).

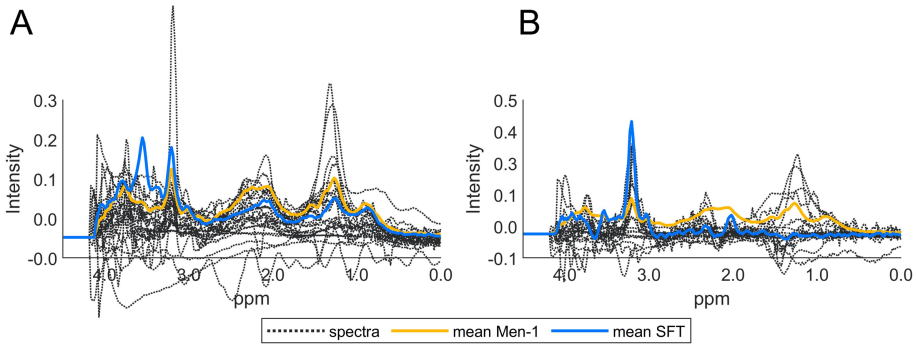

FIGURE 5 | Superimposed spectra of suboptimal quality cases. (A) Short echo (SE). (B) Long echo (LE).

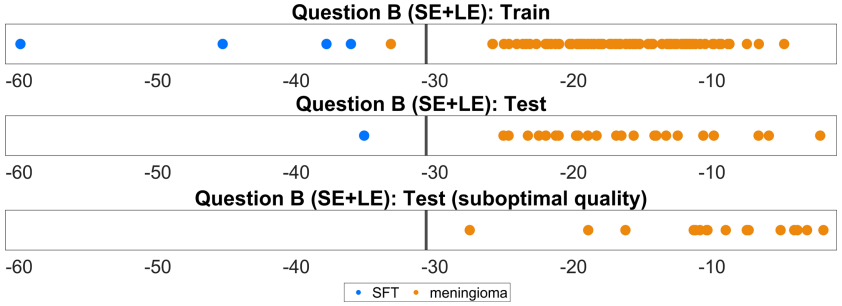

FIGURE 6 | Classification results for training, test, and suboptimal meningioma (Men) cases ($n = 21$) in the test set for Question B.

10991492, 2025, 5, Downloaded from https://analyticalsciencejournals.onlinelibrary.wiley.com/doi/10.1002/nbm.70032 by Fundació I-CERCA Fundació Institució Centres de Recerca de Catalunya, Wiley Online Library on [10/06/2025]. See the Terms and Conditions (https://onlinelibrary.wiley.com/terms-and-conditions) on Wiley Online Library for rules of use; OA articles are governed by the applicable Creative Commons License

($n = 5$) were below that age (38.6 years on average). Our results highlight the importance for clinicians to consider SFTs in patients older than 45.

Ohba et al.'s study did not identify distinguishing factors between Men-1 and Men-2. Through our study with a larger cohort and additional Men-3 cases, we found several evidences, from the classification point of view, pointing towards a continuum of the intensities for various peaks, between Men-1 and Men-3, with increasing mobile lipids and macromolecules from lower to higher grade (Figure 2). The results differentiating between Men-1 and Men-2 indicate a failure based on AUC and BER values.

It should be pointed out that the distinction of Men-1 versus Men-2 of Question C, using both TEs has an AUC of 0.666 in the test set. For Question D, the AUC of Men-1 in the test set, again using both TEs, is 0.698. From this point of view, our results represent an improvement with respect to the described performances in the distinction of Men-1 and Men-2 by conventional imaging [14, 15] and would be comparable to more sophisticated methodologies like those used in [17, 18]. Notably, two TEs are required, as with only one TE, the AUCs measures are below 0.50. These results would prompt future studies to assess the discriminative potential of using multiparametric data such as MRS together with other imaging modalities for meningioma grade discrimination.

Finally, any user can test our pipeline with their own data. Testing it only requires to install the jMRUI2XML plugin, which can be downloaded free of charge from [23] and process a short TE spectrum (TE = 30–32 ms) acquired with either 1.5- or 3-T scanners. Since our dataset is mostly composed of spectra at TR = 2000 ms and voxel sizes 3–8 cm^3, we recommend to use these parameters as well. The spectrum in this way can be entered into the prototype decision-support system accompanying this work as Supporting Information or in [32]. This prototype interface has the preloaded discrimination equation and metadata for the cases we analyzed in Question B, that is, SFT versus all meningioma and can be used in any standard computer.

Potential limitations in generalizability, such as differences in acquisition protocols and scanner field strength, should be offset by our robust processing pipeline based on the INTERPRET parameters and unit length normalization, which have demonstrated to be robust against variations in the magnetic field (1.5/3 T) or slightly different acquisition conditions [35]. With regard to the limitation in generalizability in different patient populations, it remains to be tested, which can be done with our prototype interface.

SFTs are caused by a NAB2-STAT6 gene fusion event. Both NAB2 and STAT6 are located in Chromosome 12, and are transcribed in opposite directions. The fusion event transforms a transcriptional repressor (NAB2) into a transcriptional activator (NAB2-STAT6), which in turn induces EGR1 and its downstream signaling pathways, driving neoplastic progression [36]. The NAB2-STAT6 gene fusion is pathognomic of SFTs in any part of the body. There are different variants of NAB2-STAT6 fusions, and in extrameningeal SFTs, the variants have been reported to be associated to distinct clinicopathological characteristics and prognosis [37].

Myoinositol is synthesized from Glucose-6P by Inositol-3-phosphate Synthase 1 (ISYNA1 [EC 5.5.1.4]), which converts glucose-6P to inositol-3P and Inositol Monophosphatase 1 (IMPA1 [EC 3.1.3.25] or IMPase 1), which dephosphorylates inositol-3P to form myoinositol.

The CDP-Diacylglycerol–Inositol 3-Phosphatidyltransferase (CDIPT [EC 2.7.8.11]) or Phosphatidylinositol Synthase (PIS) can use inositol to synthesize lipid phosphatidylinositol (PI). However, it is still unclear which is the origin of the myoinositol pool that regulates osmolarity, as three different symporters have been described: sodium symporters SMIT1 and SMIT2, and proton symporter HMIT. Both synthesis and transport have been reported to be regulated by osmotic stress (ISYNA1 and SMIT1, respectively). On the other hand, little is known about myoinositol degradation pathways [38].

The nature of the connection between the NABT-STAT6 fusion event and the observed myoinositol increase observed in SFTs of the brain is largely unknown nowadays. Also, to our knowledge, there are no reports on MRS of SFTs in other parts of the body. Exploring the metabolism of SFTs further, particularly the link between myoinositol regulation and NAB2-STAT6, could provide insights into the biology of SFTs and potentially uncover novel therapeutic targets.

5 | Conclusions

The detection of myoinositol, with its resonance centered at 3.52 ppm, which nearly disappears at LE, is crucial for the presurgical identification of SFTs. Differentiating between meningioma grades remains a significant challenge; however, employing two echo times improves the distinction between Grade 1 (Men-1) and Grade 2 (Men-2) meningiomas beyond random chance. In cases of poor spectral quality, the use of two echo times is advisable. Additionally, patients' age should not be considered a reliable predictor for identifying SFTs, in contrast to previous literature.

Acknowledgments

Proyectos de investigación en salud 2020, grant numbers PI20/00064 and PI20/00360. *Instituto de Salud Carlos III (ISCIII)*, Spanish *Ministerio de Economía y Competitividad*, SAF2014-52332-R. *Centro de Investigación Biomédica en Red en Bioingeniería, Biomateriales y Nanomedicina* (CIBER-BBN, http://www.ciber-bbn.es/en, accessed November 7, 2024), CB06/01/0010, an initiative of the *Instituto de Salud Carlos III* (Spain) co-funded by EU *Fondo Europeo de Desarrollo Regional* (FEDER). *Generalitat de Catalunya*, Xartecsalut, 2021 XARDI 00021. Lili Tóth was a recipient of the B21P0049 predoctoral fellowship from UAB.

Conflicts of Interest

The authors declare no conflicts of interest.

Data Availability Statement

The data that support the findings of this study are available on request from the corresponding author. The raw data are not publicly available due to privacy or ethical restrictions.

10991492, 2025, 5, Downloaded from https://analyticalsciencejournals.onlinelibrary.wiley.com/doi/10.1002/nbm.70032 by Fundació Institució Centres de Recerca de Catalunya, Wiley Online Library on [10/06/2025]. See the Terms and Conditions (https://onlinelibrary.wiley.com/terms-and-conditions) on Wiley Online Library for rules of use; OA articles are governed by the applicable Creative Commons License

References

1. A. G. Osborn, D. N. Louis, T. Y. Poussaint, L. L. Linscott, and K. L. Salzman, "The 2021 World Health Organization Classification of Tumors of the Central Nervous System: What Neuroradiologists Need to Know," *American Journal of Neuroradiology* 43, no. 7 (2022): 928–937, https://doi.org/10.3174/ajnr.A7462.

2. D. N. Louis, A. Perry, G. Reifenberger, et al., "The 2016 World Health Organization Classification of Tumors of the Central Nervous System: A Summary," *Acta Neuropathologica* 131, no. 6 (2016): 803–820, https://doi.org/10.1007/s00401-016-1545-1.

3. E. Galanis, J. C. Buckner, B. W. Scheithauer, D. W. Kimmel, P. J. Schomberg, and D. G. Piepgras, "Management of Recurrent Meningeal Hemangiopericytoma," *Cancer* 82, no. 10 (1998): 1915–1920, https://doi.org/10.1002/(SICI)1097-0142(19980515)82:10<1915::AID-CNCR15>3.0.CO;2-W.

4. A. B. Smith, I. Horkanyne-Szakaly, J. W. Schroeder, and E. J. Rushing, "From the Radiologic Pathology Archives: Mass Lesions of the Dura: Beyond Meningioma—Radiologic-Pathologic Correlation," *Radiographics* 34, no. 2 (2014): 295–312, https://doi.org/10.1148/rg.342130075.

5. T. H. Nhung, V. L. Minh, N. L. Lam, N. D. Lien, and N. M. Duc, "Malignant Intracranial Solitary Fibrous Tumor: A Case Report and Literature Review," *Radiology Case Reports* 18, no. 5 (2023): 2014–2018, https://doi.org/10.1016/j.radcr.2023.02.064.

6. T. Chikasue, Y. Uchiyama, S. Tanoue, S. Komaki, Y. Sugita, and T. Abe, "Intracranial Solitary Fibrous Tumor/Hemangiopericytoma Mimicking Cystic Meningioma: A Case Report and Literature Review," *Radiology Case Reports* 16, no. 7 (2021): 1637–1642, https://doi.org/10.1016/j.radcr.2021.04.008.

7. Y. Meng, W. Chaohu, L. Yi, P. Jun, and Q. Songtao, "Preoperative Radiologic Characters to Predict Hemangiopericytoma From Angiomatous Meningioma," *Clinical Neurology and Neurosurgery* 138 (2015): 78–82, https://doi.org/10.1016/j.clineuro.2015.08.005.

8. I. Barba, A. Moreno, I. Martinez-Pérez, et al., "Magnetic Resonance Spectroscopy of Brain Hemangiopericytomas: High Myoinositol Concentrations and Discrimination From Meningiomas," *Journal of Neurosurgery* 94, no. 1 (2001): 55–60, https://doi.org/10.3171/jns.2001.94.1.0055.

9. S. Ohba, K. Murayama, Y. Nishiyama, et al., "Clinical and Radiographic Features for Differentiating Solitary Fibrous Tumor/Hemangiopericytoma From Meningioma," *World Neurosurgery* 130 (2019): e383–e392, https://doi.org/10.1016/j.wneu.2019.06.094.

10. J. Watts, G. Box, A. Galvin, P. Brotchie, N. Trost, and T. Sutherland, "Magnetic Resonance Imaging of Meningiomas: A Pictorial Review," *Insights Into Imaging* 5, no. 1 (2014): 113–122, https://doi.org/10.1007/s13244-013-0302-4.

11. N. A. Sibtain, F. A. Howe, and D. E. Saunders, "The Clinical Value of Proton Magnetic Resonance Spectroscopy in Adult Brain Tumours," *Clinical Radiology* 62, no. 2 (2007): 109–119, https://doi.org/10.1016/j.crad.2006.09.012.

12. C. Majós, J. Alonso, C. Aguilera, et al., "Utility of Proton MR Spectroscopy in the Diagnosis of Radiologically Atypical Intracranial Meningiomas," *Neuroradiology* 45, no. 3 (2003): 129–136, https://doi.org/10.1007/s00234-002-0933-5.

13. V. Yarabarla, A. Mylarapu, T. J. Han, S. L. McGovern, S. M. Raza, and T. H. Beckham, "Intracranial Meningiomas: An Update of the 2021 World Health Organization Classifications and Review of Management With a Focus on Radiation Therapy," *Frontiers in Oncology* 13 (2023): 1137849, https://doi.org/10.3389/fonc.2023.1137849.

14. M. Julià-Sapé, D. Acosta, C. Majós, et al., "Comparison Between Neuroimaging Classifications and Histopathological Diagnoses Using an International Multicenter Brain Tumor Magnetic Resonance Imaging Database," *JNS* 105, no. 1 (2006): 6–14, https://doi.org/10.3171/jns.2006.105.1.6.

15. K. Arita, M. Miwa, M. Bohara, F. Moinuddin, K. Kamimura, and K. Yoshimoto, "Precision of Preoperative Diagnosis in Patients With Brain Tumor—A Prospective Study Based on "Top Three List" of Differential Diagnosis for 1061 Patients," *Surgical Neurology International* 11 (2020): 55, https://doi.org/10.25259/SNI_5_2020.

16. Y. Yao, Y. Xu, S. Liu, et al., "Predicting the Grade of Meningiomas by Clinical–Radiological Features: A Comparison of Precontrast and Postcontrast MRI," *Frontiers in Oncology* 12 (2022): 1053089, https://doi.org/10.3389/fonc.2022.1053089.

17. M. Panigrahi, N. K. Bodhey, S. K. Pati, N. Hussain, A. K. Sharma, and A. K. Shukla, "Differentiation Between Various Types and Subtypes of Intracranial Meningiomas With Advanced MRI," *South African Journal of Radiology* 26, no. 1 (2022): 2480, https://doi.org/10.4102/sajr.v26i1.2480.

18. A. Vassantachart, Y. Cao, M. Gribble, et al., "Automatic Differentiation of Grade I and II Meningiomas on Magnetic Resonance Image Using an Asymmetric Convolutional Neural Network," *Scientific Reports* 12, no. 1 (2022): 3806, https://doi.org/10.1038/s41598-022-07859-0.

19. LCModel's Home Page. Accessed November 20, 2023, http://s-provencher.com/lcmodel.shtml.

20. Organisation Mondiale de la Santé, Centre International de Recherche sur le Cancer, ed., *Central Nervous System Tumours*, 5th ed. (International Agency for Research on Cancer, 2021).

21. D. Stefan, F. D. Cesare, A. Andrasescu, et al., "Quantitation of Magnetic Resonance Spectroscopy Signals: The jMRUI Software Package," *Measurement Science and Technology* 20, no. 10 (2009): 104035, https://doi.org/10.1088/0957-0233/20/10/104035.

22. V. Mocioiu, S. Ortega-Martorell, I. Olier, et al., "From Raw Data to Data-Analysis for Magnetic Resonance Spectroscopy—The Missing Link: jMRUI2XML," *BMC Bioinformatics* 16, no. 1 (2015): 378, https://doi.org/10.1186/s12859-015-0796-5.

23. JMRUI2XML Plugin for jMRUI (Software), https://doi.org/10.34810/data1497.

24. M. van der Graaf, M. Julià-Sapé, F. A. Howe, et al., "MRS Quality Assessment in a Multicentre Study on MRS-Based Classification of Brain Tumours," *NMR in Biomedicine* 21, no. 2 (2008): 148–158, https://doi.org/10.1002/nbm.1172.

25. A. R. Tate, J. Underwood, D. M. Acosta, et al., "Development of a Decision Support System for Diagnosis and Grading of Brain Tumours Using In Vivo Magnetic Resonance Single Voxel Spectra," *NMR in Biomedicine* 19, no. 4 (2006): 411–434, https://doi.org/10.1002/nbm.1016.

26. H. Barkhuijsen, R. de Beer, and D. van Ormondt, "Improved Algorithm for Noniterative Time-Domain Model Fitting to Exponentially Damped Magnetic Resonance Signals," *Journal of Magnetic Resonance* 73, no. 3 (1987): 553–557, https://doi.org/10.1016/0022-2364(87)90023-0.

27. W. W. F. Pijnappel, A. van den Boogaart, R. de Beer, and D. van Ormondt, "SVD-Based Quantification of Magnetic Resonance Signals," *Journal of Magnetic Resonance* 97, no. 1 (1992): 122–134, https://doi.org/10.1016/0022-2364(92)90241-X.

28. J. M. García-Gómez, S. Tortajada, C. Vidal, et al., "The Effect of Combining Two Echo Times in Automatic Brain Tumor Classification by MRS," *NMR in Biomedicine* 21, no. 10 (2008): 1112–1125, https://doi.org/10.1002/nbm.1288.

29. S. Ortega-Martorell, I. Olier, M. Julià-Sapé, and C. Arús, "SpectraClassifier 1.0: A User Friendly, Automated MRS-Based Classifier-Development System," *BMC Bioinformatics* 11, no. 1 (2010): 106, https://doi.org/10.1186/1471-2105-11-106.

30. A. P. Candiota, C. Majós, A. Bassols, et al., "Assignment of the 2.03 ppm Resonance in In Vivo 1H MRS of Human Brain Tumour Cystic Fluid: Contribution of Macromolecules," *Magma* 17, no. 1 (2004): 36–46, https://doi.org/10.1007/s10334-004-0043-y.

10991492, 2025, 5, Downloaded from https://analyticalsciencejournals.onlinelibrary.wiley.com/doi/10.1002/nbm.70032 by Fundació I-CERCA Fundació Institució Centres de Recerca de Catalunya, Wiley Online Library on [10/06/2025]. See the Terms and Conditions (https://onlinelibrary.wiley.com/terms-and-conditions) on Wiley Online Library for rules of use; OA articles are governed by the applicable Creative Commons License

31. V. Govindaraju, K. Young, and A. A. Maudsley, "Proton NMR Chemical Shifts and Coupling Constants for Brain Metabolites," *NMR Biomed*. 13, no. 3 (2000): 129–153, https://doi.org/10.1002/1099-1492(200005)13:3<129::AID-NBM619>3.0.CO;2-V.

32. L. F. Tóth, C. Arus, C. Majos, A. Pons-Escoda, and M. Julià-Sapé, Meningioma-SFT-Classifier (Software) (Version 1.0). CORA.Repositori de Dades de Recerca. 2025, https://doi.org/10.34810/DATA2109.

33. R. Kreis, "Issues of Spectral Quality in Clinical 1H-Magnetic Resonance Spectroscopy and a Gallery of Artifacts," *NMR in Biomedicine* 17, no. 6 (2004): 361–381, https://doi.org/10.1002/nbm.891.

34. J. Martin-Broto, J. L. Mondaza-Hernandez, D. S. Moura, and N. Hindi, "A Comprehensive Review on Solitary Fibrous Tumor: New Insights for New Horizons," *Cancers (Basel)* 13, no. 12 (2021): 2913, https://doi.org/10.3390/cancers13122913.

35. M. Julià-Sapé, J. R. Griffiths, R. A. Tate, et al., "Classification of Brain Tumours From MR Spectra: The INTERPRET Collaboration and Its Outcomes: Robust Classification of Brain Tumours From MR Spectra," *NMR in Biomedicine* 28, no. 12 (2015): 1772–1787, https://doi.org/10.1002/nbm.3439.

36. D. R. Robinson, Y. M. Wu, S. Kalyana-Sundaram, et al., "Identification of Recurrent NAB2-STAT6 Gene Fusions in Solitary Fibrous Tumor by Integrative Sequencing," *Nature Genetics* 45, no. 2 (2013): 180–185, https://doi.org/10.1038/ng.2509.

37. T. Georgiesh, H. M. Namløs, N. Sharma, et al., "Clinical and Molecular Implications of NAB2-STAT6 Fusion Variants in Solitary Fibrous Tumour," *Pathology* 53, no. 6 (2021): 713–719, https://doi.org/10.1016/j.pathol.2020.11.010.

38. X. B. Su, A. L. A. Ko, and A. Saiardi, "Regulations of myo-Inositol Homeostasis: Mechanisms, Implications, and Perspectives," *Advances in Biological Regulation* 87 (2023): 100921, https://doi.org/10.1016/j.jbior.2022.100921.

Supporting Information

Additional supporting information can be found online in the Supporting Information section.

10991492, 2025, 5, Downloaded from https://analyticalsciencejournals.onlinelibrary.wiley.com/doi/10.1002/nbm.70032 by Fundació Institució Centres de Recerca de Catalunya, Wiley Online Library on [10/06/2025]. See the Terms and Conditions (https://onlinelibrary.wiley.com/terms-and-conditions) on Wiley Online Library for rules of use; OA articles are governed by the applicable Creative Commons License